JOURNAL OF MATERIALS SCIENCE 22 (1987) 449–458

Influence of ion implantation on the microstructure of oxide scales formed on a 20Cr/25Ni/Nb-stabilized stainless steel in carbon dioxide at 825° C

C. H. YANG, P.A. LABUN, G. WELSCH, T. E. MITCHELL
Department of Metallurgy and Materials Science, Case Institute of Technology, Case Western Reserve University, Cleveland, Ohio 44106, USA

M. J. BENNETT
Materials Development Division, B. 393, AERE, Harwell, Didcot, Oxfordshire OX11 ORA, UK

Specimens of a stainless steel (20% Cr, 25% Ni stabilized with niobium and also containing 0.9% Mn and 0.6% Si) implanted with lanthanum to a dose of 10^{17} ion cm^{-2}, together with unimplanted specimens, have been oxidized in carbon dioxide at 825° C for times up to 9735 h. Transverse sections through the oxide scales formed on the respective specimens have been studied by analytical electron microscopy. After this exposure the scale on the unimplanted 20/25/Nb stainless steel consists of an outer, large-grained, spinel layer, a middle fine-grained Cr_2O_3 layer and an inner, discontinuous silicon rich, niobium and chromium bearing, amorphous layer. The main effects of the lanthanum implantation are to improve oxidation resistance and maintain scale adherence during thermal cycling. The microstructural changes in the scale formed on the lanthanum implanted 20/25/Nb steel include finer Cr_2O_3 oxide grains and an intermediate region between the outer spinel and inner Cr_2O_3 layers comprised of both oxides. The lanthanum concentrates in this region and appears to act as a marker due to its low diffusivity. Mechanisms of scale development on the 20/25/Nb stainless steel and the influence of lanthanum implantation are discussed.

1. Introduction

Minor additions of reactive elements, such as yttrium and the rare earths, to Ni–Cr and Fe–Ni–Cr alloys play a crucial role in improving the behaviour of scales formed during oxidation, as described, for example, by Stott *et al.* [1] and Bennett *et al.* [2], respectively. The improvement manifests itself firstly, by reducing the extent of attack and secondly, by improving the scale adhesion under thermal cycling conditions. The reactive elements can be added through the bulk by alloying or specifically at the surface by ion implantation.

Several mechanisms have been proposed to account for the improvements:

1. the reactive elements in the surface act as nucleation sites for the protective Cr_2O_3 layer, thus increasing its rate of formation [3, 4];
2. the reactive elements form a blocking layer, which reduces the outward cation diffusion rate and minimizes any depletion of the scale-forming elements within the substrate [5, 6];
3. the large size of the reactive elements causes them to act as sinks for vacancies and, therefore, to decrease the number of voids at the interface [7, 8];
4. the incorporation of the reactive elements changes the physico-chemical properties (e.g. plasticity) of the scale so that strain can be accommodated by deformation rather than cracking [9];
5. the reactive elements modify the predominant scale growth mechanism.

Most studies have concentrated on gravimetric measurements to evaluate oxidation and spallation kinetics. In addition, electron probe microanalysis (EMPA), scanning electron microscopy (SEM) and X-ray diffraction (XRD) have been used to characterize the scale macrostructure and chemical constituents. Such techniques are useful but do not provide sufficient microstructural and microchemical information about the scale necessary to unravel the effects of reactive elements on the oxidation behaviour of alloys.

In the present paper, scales formed on both lanthanum-implanted and unimplanted 20/25/Nb-stabilized stainless steel have been examined using analytical electron microscopy (AEM) to elucidate the effect of rare earth elements upon the oxidation behaviour of this steel. Previous work [2] has shown that implanted europium, lanthanum and ytterbium all improve the oxidation resistance and scale adhesion during oxidation in carbon dioxide at 825° C. For the unimplanted steel the oxidation sequence consists of the initial formation of an iron-rich spinel followed by

0022–2461/87 $03.00 + .12

the successive development of a Cr_2O_3 inner layer and eventually, an underlying amorphous SiO_2 layer at the steel interface. These three layers together constitute what is termed subsequently the "uniform" protective oxide scale. Fracture within the SiO_2 layer or at the SiO_2/steel interface leads to spallation; re-oxidation of the exposed chromium-depleted steel can lead to pitting attack. Implantation of europium, lanthanum and ytterbium, as well as cerium and yttrium, decreases the overall extent of oxidation and also prevents spallation and pitting attack.

2. Experimental techniques

The 20/25/Nb steel was analysed and found to contain 19.9% Cr, 22.6% Ni, 0.9% Mn, 0.7% Nb, 0.56% Si and 0.04% C by weight. Ion implantation, at 300 keV, was carried out with the Harwell Cockcroft-Walton accelerator to a dose of 10^{17} ion cm^{-2}, giving an implanted layer thickness of about 70 nm with a Gaussian distribution of lanthanum concentration with a maximum of 32 at % at a depth of 40 nm. The specimens were oxidized at 825° C in carbon dioxide; unimplanted 20/25/Nb steel for 9735 h and lanthanum-implanted 20/25/Nb steel for 6500 h. Further details are given elsewhere [2].

Both transverse and parallel (back-thinned) sections were produced and these were ion-thinned to obtain foils for AEM examination. Transverse sections were prepared using the technique described by Tinker and Labun [10], namely by electroforming nickel onto the surface, followed by sectioning with a diamond saw, mechanical polishing and ion-milling. Back-thinned sections were obtained by ion-thinning from one side or were thinned electrochemically using a Struers Tenupol apparatus. In the latter case, a thin plastic film protected the oxide scale and only one jet was electrically connected. All thinned scale sections were examined in a Philips EM400T transmission electron microscope with comprehensive analytical facilities, including STEM (scanning transmission electron microscopy) and X-ray EDS (energy dispersive spectrometry).

3. Results

The results on unimplanted specimens will be discussed first, followed by those on lanthanum-implanted specimens.

3.1. Unimplanted 20/25/Nb stainless steel

After exposure to carbon dioxide for 9735 h at 825° C, the oxide scale was found to consist of three distinct regions: an outer spinel layer containing mostly iron and nickel with smaller amounts of chromium and manganese, a 3 to 4 μm thick Cr_2O_3 layer in the middle of the scale and an amorphous silica layer containing variable niobium and chromium concentrations near the steel substrate. This amorphous SiO_2 layer is not continuous so that the Cr_2O_3 is sometimes in direct contact with the steel. Other observations include the fine-grained nature of the Cr_2O_3 layer, porosity in the scale near the steel interface, and dislocation activity in the steel substrate; these will be described in more detail below.

The total oxide scale thickness is approximately 4.5 μm. In Fig. 1 the innermost amorphous oxide layer (a), the middle rhombohedral (Cr_2O_3) layer (b), and a portion of the outer spinel layer (c), are shown along with the corresponding EDS spectrum for each area. The niobium concentration in this region of the inner amorphous layer (a) is rather high (~ 37% Nb

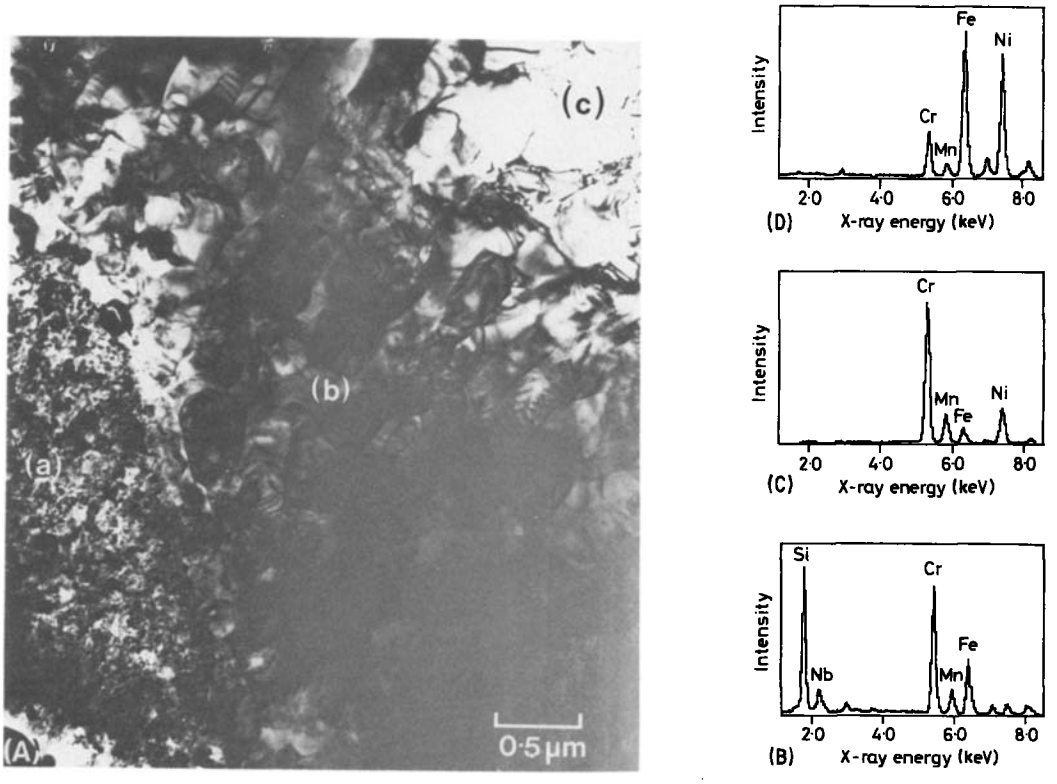

Figure 1 (A) Transmission electron bright-field micrograph from a transverse section through the oxide scale formed on unimplanted 20/25/Nb steel and (B) to (D) the EDS spectra from regions (a), (b), (c) in (A) where (a) is an inner amorphous layer, (b) is the Cr_2O_3 layer, and (c) is a spinel layer.

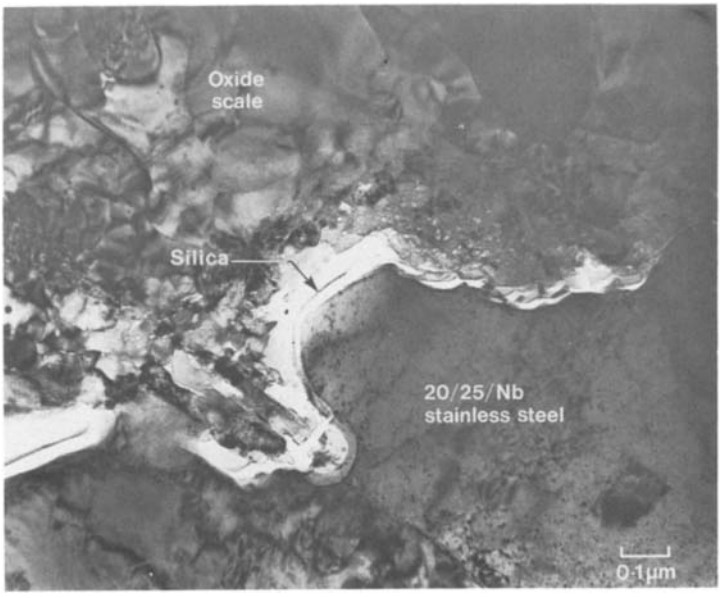

Figure 2 Transmission electron bright-field micrograph from a transverse section through the oxidized unimplanted 20/25/Nb steel showing the amorphous oxide layer at the scale/steel interface.

and 40% Si from the EDS spectrum in Fig. 1). The amorphous nature was revealed by selected-area diffraction (SAD). This layer also contained a significant but variable chromium content. In fact EDS and microdiffraction analysis showed that the higher chromium content regions tended to have some crystallinity, while the low chromium content regions were amorphous. The grains of the Cr_2O_3 layer (b) are mostly elongated ($\sim 0.5\,\mu m$ long by $\sim 0.25\,\mu m$ wide) and probably result from competitive growth of favourably oriented oxide. SAD showed that the outer layer of oxide (c), which contains mostly iron and nickel, has the spinel structure. Although the relative thickness of these three layers of the scale varied from area to area, a continuous 2 to 3 μm thick layer of Cr_2O_3 was observed consistently.

The results obtained from other areas indicate that the spinel layer is not always present over the Cr_2O_3 layer so that effectively the Cr_2O_3 layer extended to the gas/oxide interface. Since the scale is quite brittle, it is likely that the spinel layer is present initially but spalls either during an early stage of specimen preparation or during ion thinning.

Details of the interface between the steel and scale are shown in Fig. 2. In this region examined, the amorphous layer is essentially silica, is not continuous and varies in thickness. The inner portion of the Cr_2O_3 layer is fine-grained with an equiaxed structure. A high dislocation density, and a contorted structure also observed in the Cr_2O_3 layer close to the interface, are presumably caused by growth stresses.

Submicron porosity develops within the scale, as shown in Figs 3a and b and also in Fig. 2. The high porosity close to the substrate suggests that the pores are formed from vacancy agglomeration during the exchange process, while the cations diffuse outward to form the scale.

The steel immediately below the oxide has also been investigated. Dislocations arranged in subgrain boundaries are observed, as shown in Fig. 4. This implies that the steel sub-surface region has undergone creep under stress. There is also a modest density of dislocations randomly arranged inside the subgrains. These observations indicate that there are growth stresses during the formation of the oxide scale.

In summary, during the extended oxidation of the unimplanted 20/25/Nb-stabilized stainless steel a continuous layer of Cr_2O_3 with relatively uniform thickness is formed. In some regions an amorphous silicon-rich oxide with variable niobium and chromium contents is produced additionally between the Cr_2O_3 scale and the steel substrate. Also, the Cr_2O_3 layer apparently extends to the gas interface in some areas

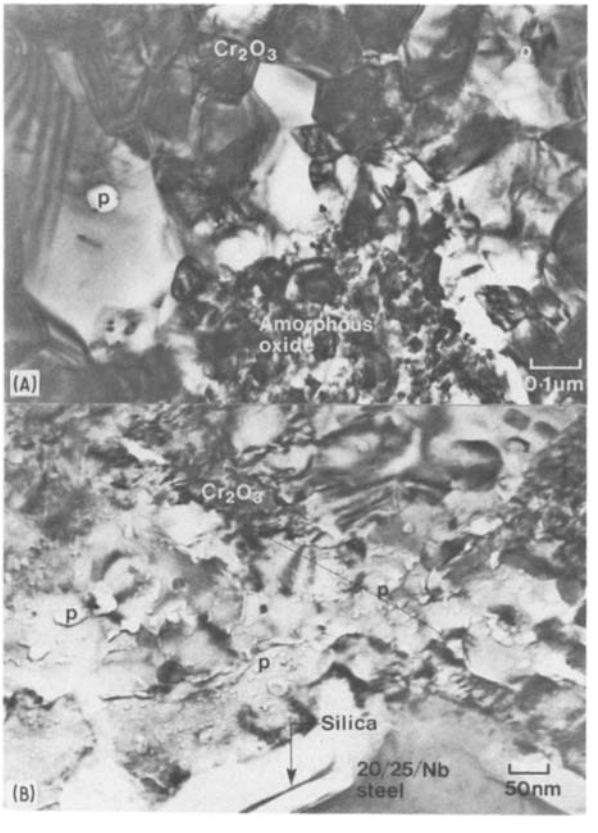

Figure 3 Transmission electron bright-field micrographs from a transverse section through the oxidized unimplanted 20/25/Nb steel showing the fine-grained equiaxed Cr_2O_3 layer with porosity (p) in it and the amorphous layer.

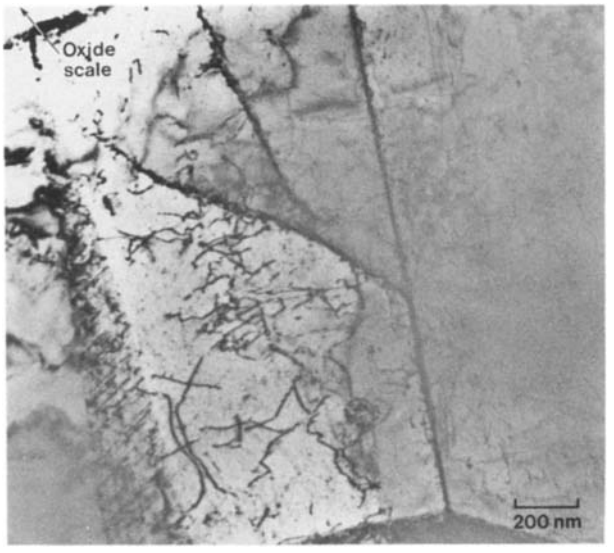

Figure 4 Transmission electron bright-field micrograph from a transverse section through the oxidized unimplanted 20/25/Nb steel showing the dislocation substructure developed in the steel near the interface with the scale.

but is usually overlain with an outer layer of (Fe, Ni) spinel.

3.2. Lanthanum-implanted 20/25/Nb stainless steel

The oxide scale on the lanthanum 20/25/Nb stainless steel was found to consist of four distinct layers: a manganese-rich spinel at the oxide–gas interface, a middle layer containing a mixture of spinel and rhombohedral oxides, an inner Cr_2O_3 layer with a very fine grain size, and a discontinuous amorphous oxide layer at the alloy interface. Details of each layer are given below. Interestingly, the strong adherence of the scale on the lanthanum-implanted specimens makes transverse sectioning through the oxide scale easier. Typical micrographs and analyses are shown in Figs 5 to 10. The dark-field image in Fig. 5 was formed using a prominent spinel reflection and reveals the multiple oxide layers. The total scale thickness is $\sim 2.5\,\mu m$ compared to an unimplanted scale thickness of $\sim 4.5\,\mu m$, confirming the gravimetric measurements [2] that lanthanum implantation greatly improves the oxidation resistance of the 20/25/Nb stainless steel.

The outermost spinel oxide layer is $\sim 1.0\,\mu m$ thick and its grain size is also $\sim 1.0\,\mu m$, as can be seen in Fig. 6, a bright-field image from the same area shown as a dark-field image in Fig. 5. EDS results, together with the corresponding micro-diffraction patterns, show that the spinel has a high manganese content.

In the middle layer of the oxide scale, which has a thickness of less than $1\,\mu m$, both rhombohedral Cr_2O_3 and cubic spinel grains are present, as determined by microdiffraction and by placing the electron probe on different grains for EDS analysis. In general, the grains of high chromium content are found to have the rhombohedral structure with a small but variable grain size of generally less than $0.5\,\mu m$; the grain size tends to decrease as the scale/steel interface is approached, while the chromium content increases (Fig. 6). The spinel grain sizes are considerably smaller than in the outermost layer.

The innermost, rhombohedral, oxide layer has a very fine grain size and a thickness of $\sim 0.05\,\mu m$. The morphology, along with the corresponding diffraction patterns from the indicated areas, is presented in Fig. 7. Many of the grains in Fig. 7 exhibit Moiré fringes. These arise from the overlap of oxide grains, which are either slightly rotated with respect to each other or oriented such as to give strong diffraction from planes of different *d*-spacing. Some elastic strain contours are also seen in the grains of Fig. 7 but no evidence of either dislocation activity or porosity is observed.

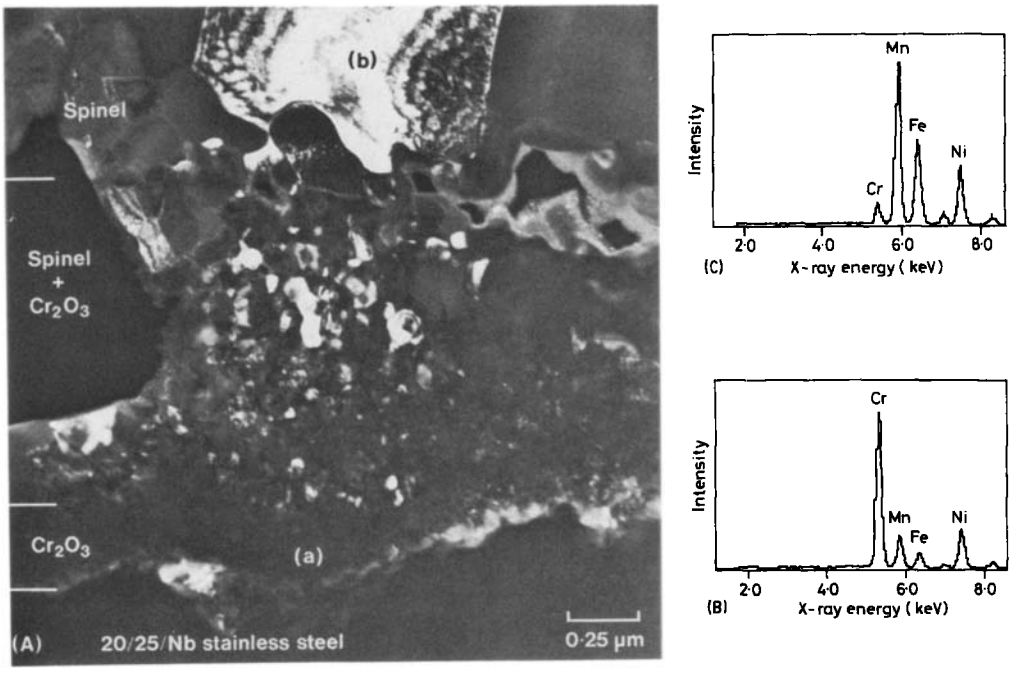

Figure 5 (A) Transmission electron dark-field (df) micrograph from a transverse section through the oxidized lanthanum-implanted 20/25/Nb steel showing the three oxide layers, together with the EDS spectra from (B) region (a) Cr_2O_3, and (C) region (b) spinel.

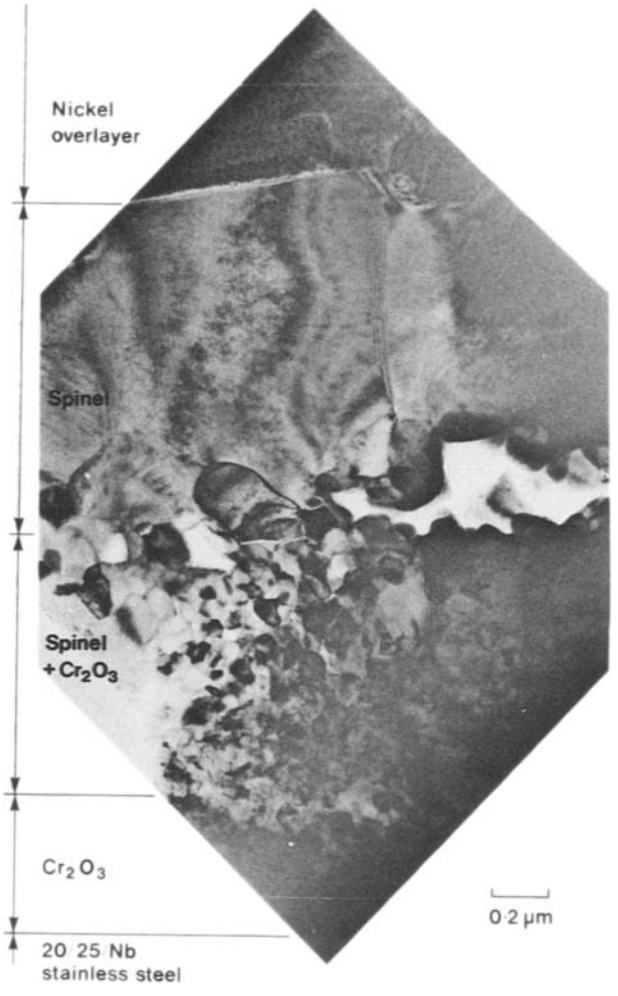

Figure 6 Transmission electron bright-field micrograph from a transverse section through the oxide scale formed on lanthanum-implanted 20/25/Nb steel showing the large grains of spinel compared with the finer grains of Cr_2O_3 and spinel.

The large voids and cracks present between the intermediate layer and the outermost layer of the scale (Fig. 6) are probably artefacts resulting from preferential thinning of particular grains by the ion beam during the specimen preparation.

Fig. 8 shows a composite micrograph along several micrometres of scale/steel interface, revealing that the boundary is highly irregular. Furthermore, the interface is delineated in some areas by a silica layer, as shown in the high magnification bright-field image of Fig. 9. The corresponding microdiffraction pattern (Fig. 9b) taken of the silica layer shows it to be amorphous.

The location of the lanthanum was investigated by EDS techniques and it was found to be concentrated in grains in the middle of the scale at the interface with the outer spinel layer. A bright-field STEM micrograph and a lanthanum ($L\alpha$) X-ray map are presented in Figs 10a and b, respectively. The EDS spectrum and the microdiffraction pattern of a typical grain with a high lanthanum concentration are shown in Figs 10c and d, respectively. Fig. 10b shows that there is a continuous band of oxide grains with a high concentration of lanthanum in the middle of the scale, adjacent to the outer spinel region. Fig. 10c indicates that the concentration of lanthanum is comparable with that of chromium, manganese, iron and nickel, while Fig. 10d establishes that these grains have the cubic spinel structure. It should be emphasized that, in all cases, the lanthanum was detected inside the spinel grains. There was no evidence of either La_2O_3 or $LaFeO_3$ existing in the scale.

4. Discussion

A uniform and protective scale forms on unimplanted 20/25/Nb stainless steel when oxidized for 4900 h at 825° C, as has been reported previously [11]. In consists of an outer $MnCr_2O_4$ spinel oxide layer, a middle layer of fine, equiaxed Cr_2O_3 and an inner ~ 20 nm thick continuous amorphous SiO_2 layer (see Fig. 11). The oxide grows via outward cation movement. The high oxygen affinity of manganese accounts for the formation of the outer manganese-rich spinel. The present investigation of scale formed on the same steel oxidized at 825° C for longer times (9735 h) shows that the scale has changed in two important ways: the inner amorphous layer is not continuous and the outer spinel contains high concentrations of iron and nickel. Apparently extensive spallation of the initially formed uniform scale and subsequent internal pitting attack has occurred during the longer time of oxidation. Because of the chromium-depletion in the underlying stainless steel, the new oxide that forms after spallation on reoxidation is different from the initially formed scale and therefore, it is not surprising to find high concentration of iron and nickel in the outer spinel until an inner protective Cr_2O_3 layer can be re-established [12, 13]. The formation at the steel interface of a silicon-rich, niobium-bearing oxide is due to the high oxygen affinity of these elements at low oxygen partial pressure.

The lanthanum-implanted 20/25/Nb stainless steel develops a scale similar to the uniform scale on the unimplanted steel. It contains the three layers of spinel, chromium sesquioxide and silica. Thus, physical effects resulting from ion implantation do not influence the scale growth. However, there are a number of differences including: (1) there is no sharp delineation of the spinel and chromium sesquioxide layers; (2) the silica layer is discontinuous; (3) growth of the scale apparently results from inward, as well as outward, diffusion processes, suggesting that lanthanum-implantation causes a change in the growth mechanism; (4) the adherence of the oxide scale is greatly enhanced. Each of these aspects will be discussed in detail below.

4.1. The 20/25/Nb stainless steel oxidation sequence

A microstructural sequence for the oxidation of 20/25/Nb stainless steel appears to be as follows. At the beginning of the reaction, $(Fe, Cr, Ni)_3O_4$ spinel nucleates on the steel surface and contains concentrations of iron, chromium and nickel roughly in proportion to those in the steel. The manganese, which is more reactive than chromium with oxygen, subsequently diffuses to the steel/oxide interface and concentrates in the outer spinel oxide.

The oxygen activity beneath the spinel layer is low but sufficient to form Cr_2O_3; therefore, a protective

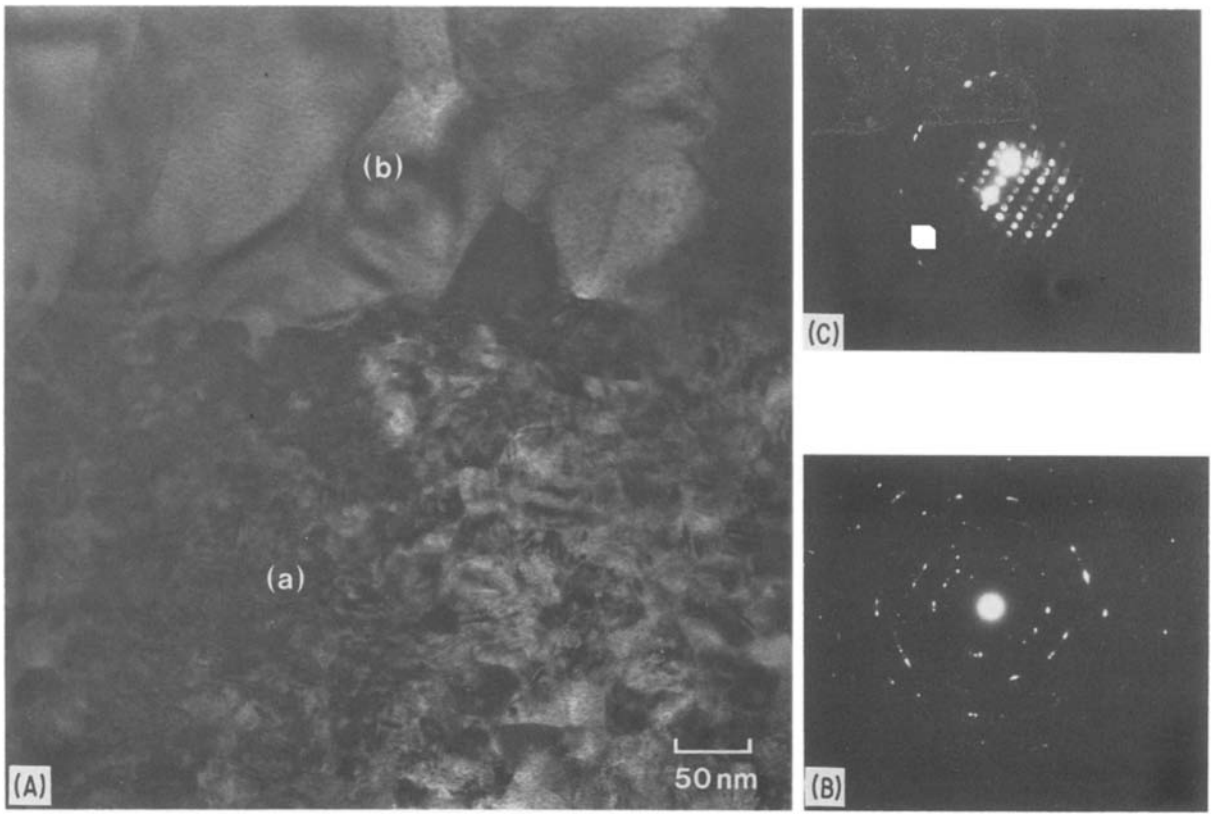

Figure 7 (A) Transmission electron bright-field micrograph from the oxidized lanthanum-implanted 20/25/Nb steel showing the fine-grained chromium-rich inner oxide layer (a) and the middle layer (b), together with (B) the corresponding SADP from region (a), and (C) the microdiffraction pattern from region (b).

film of Cr_2O_3 is produced by the outward diffusion of chromium. The formation of Cr_2O_3 on the steel establishes an even lower oxygen partial pressure at the oxide/steel interface. Once this pressure is established by a continuous layer of Cr_2O_3, SiO_2 will be the only stable oxide phase that can form at such low partial pressures. In fact, as pointed out by Bennett *et al.* [12], the inner oxide layers are probably produced by interdiffusion and solid state reactions: the Cr_2O_3 by a reaction between chromium from the steel with the spinel oxide and the SiO_2 by a reaction between silicon from the alloy with the Cr_2O_3. Fig. 12a is a schematic illustration of the fully developed, uniform protective scale formed on 20/25/Nb stainless steel.

4.2. Reoxidation after spallation

Spalling is initiated either at the SiO_2 steel interface or within the continuous SiO_2 layer itself [12]. As pointed out earlier, the alloy surface becomes depleted in chromium; therefore the oxide which forms after spallation will be of a different character than the uniform scale [12, 13]. The first oxide nucleated after spallation will be a spinel, enriched in iron and nickel, with a concentration roughly proportional to that in the

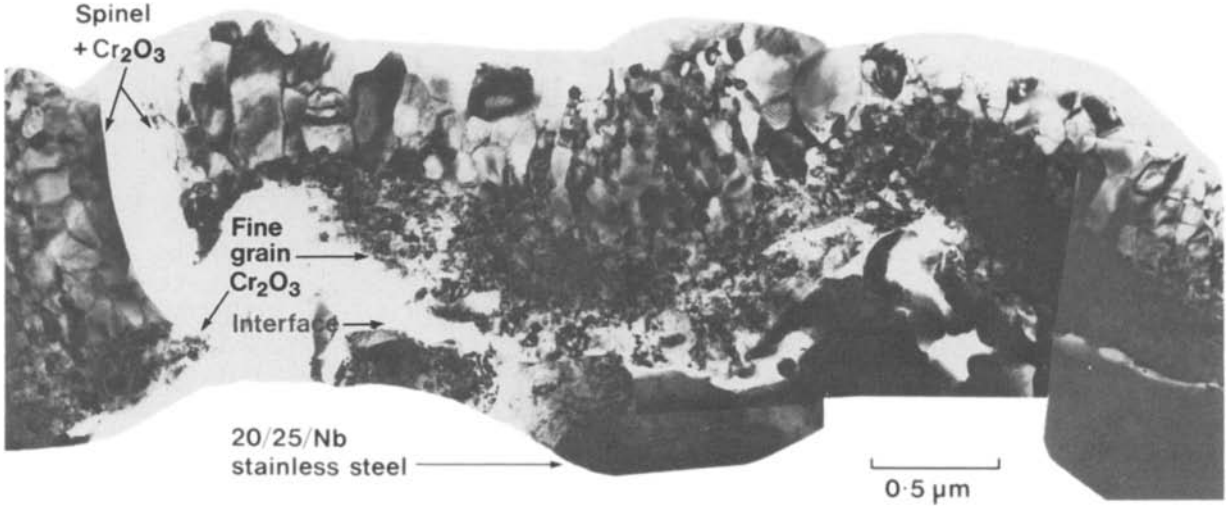

Figure 8 Composite of transmission electron bright-field micrographs from an oxidized lanthanum-implanted 20/25/Nb steel showing the irregular interface between the steel and the oxide scale.

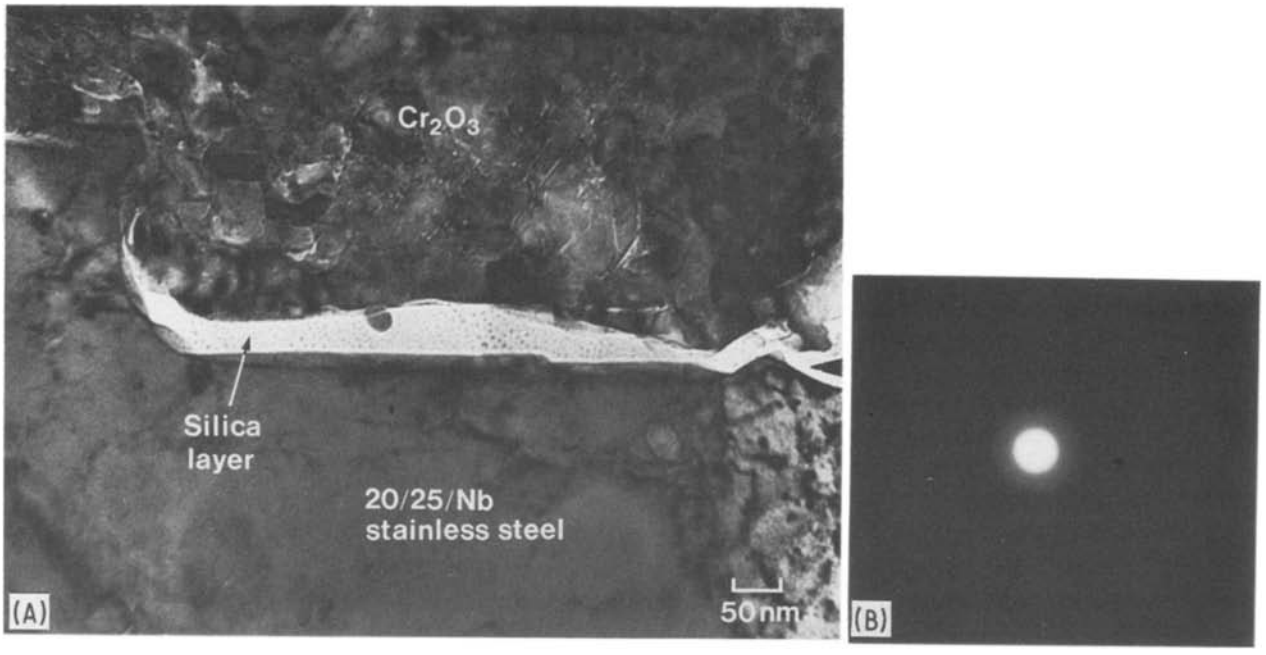

Figure 9 (A) Transmission electron bright-field micrograph of oxidized lanthanum-implanted 20/25/Nb steel showing the discontinuous silica layer at the steel/scale interface; (B) corresponding microdiffraction pattern from the amorphous silica.

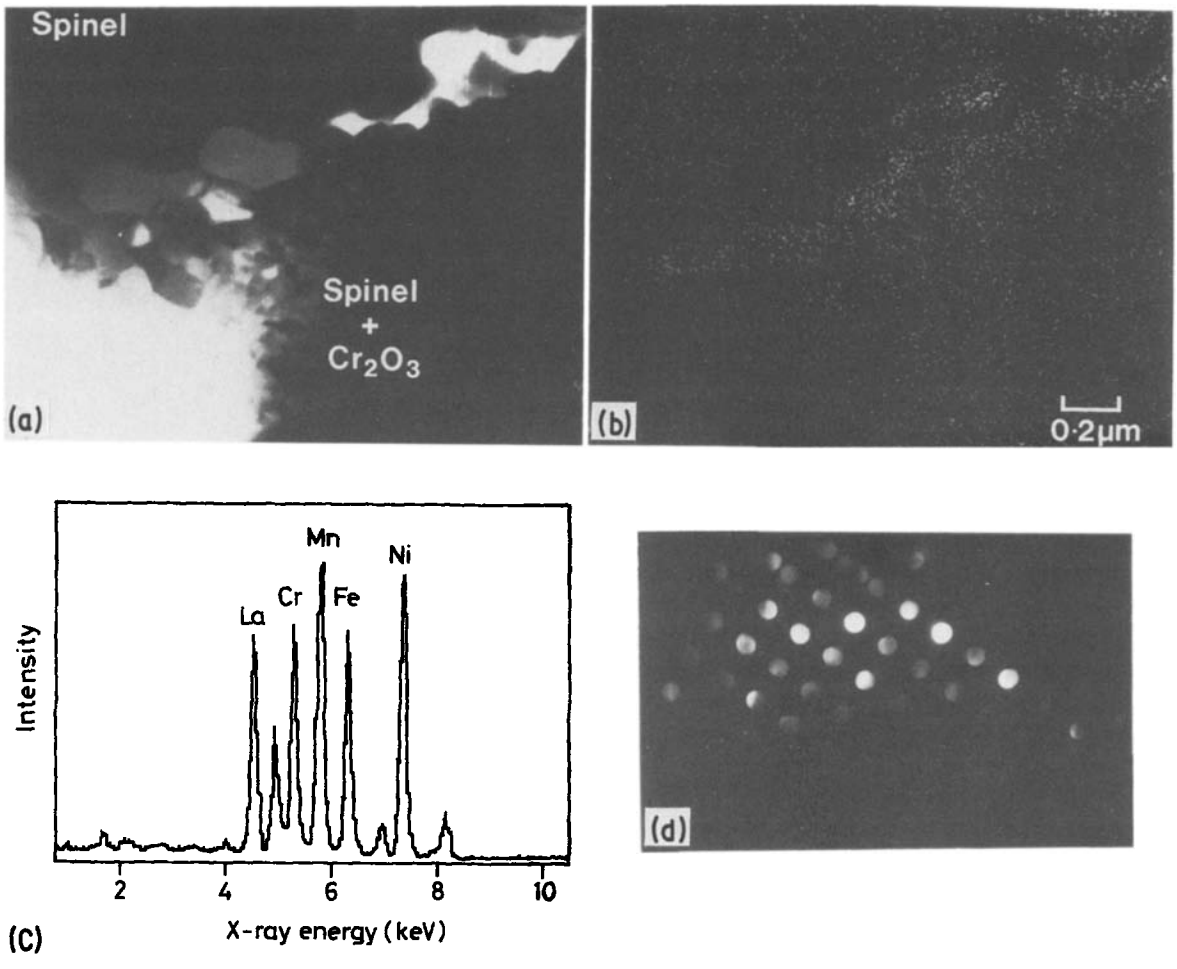

Figure 10 (A) STEM bright-field micrograph from oxidized lanthanum-implanted 20/25/Nb steel showing the region between the outer spinel oxide and the intermediate layer; (B) a lanthanum *Lα* map of the same region as in (A); (C) an EDS spectrum from a lanthanum-rich grain; (D) microdiffraction pattern from a lanthanum-rich grain.

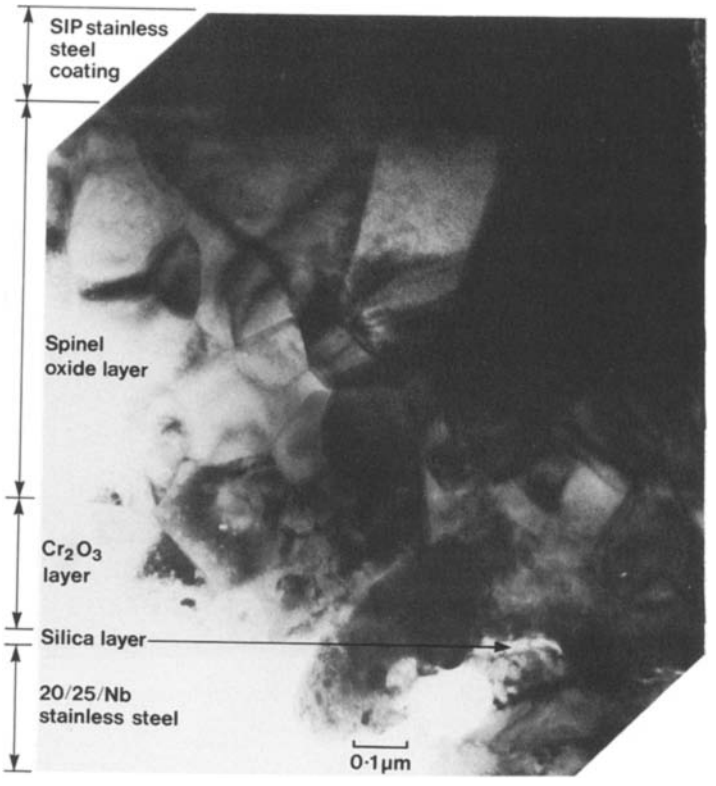

Figure 11 Transmission electron bright-field micrograph of the uniform oxide scale formed on unimplanted 20/25/Nb stainless steel during 4900 h oxidation in carbon dioxide at 825° C showing a continuous silica layer at the steel/scale interface (from [11]).

steel. Subsequent growth occurs by both outward cation and inward anion movement. When sufficient chromium is present, a healing layer of Cr_2O_3 will reform beneath the iron-rich spinel. Once again, a low oxygen partial pressure will exist at the steel/oxide interface, permitting the formation of a silicon-rich oxide. However, this layer is discontinuous. The schematic illustration of this type of scale is shown in Fig. 12b.

4.3. Modification of the growth mechanism by implanted lanthanum

Since the radius of the La^{3+} ion is about 50% larger than the other alloying elements in the stainless steel, it is likely that its diffusion rate will be very slow, relative to the other elements. This applies to diffusion in both the alloy and the oxide scale. The depth of the implanted region is oxidized within one hour of

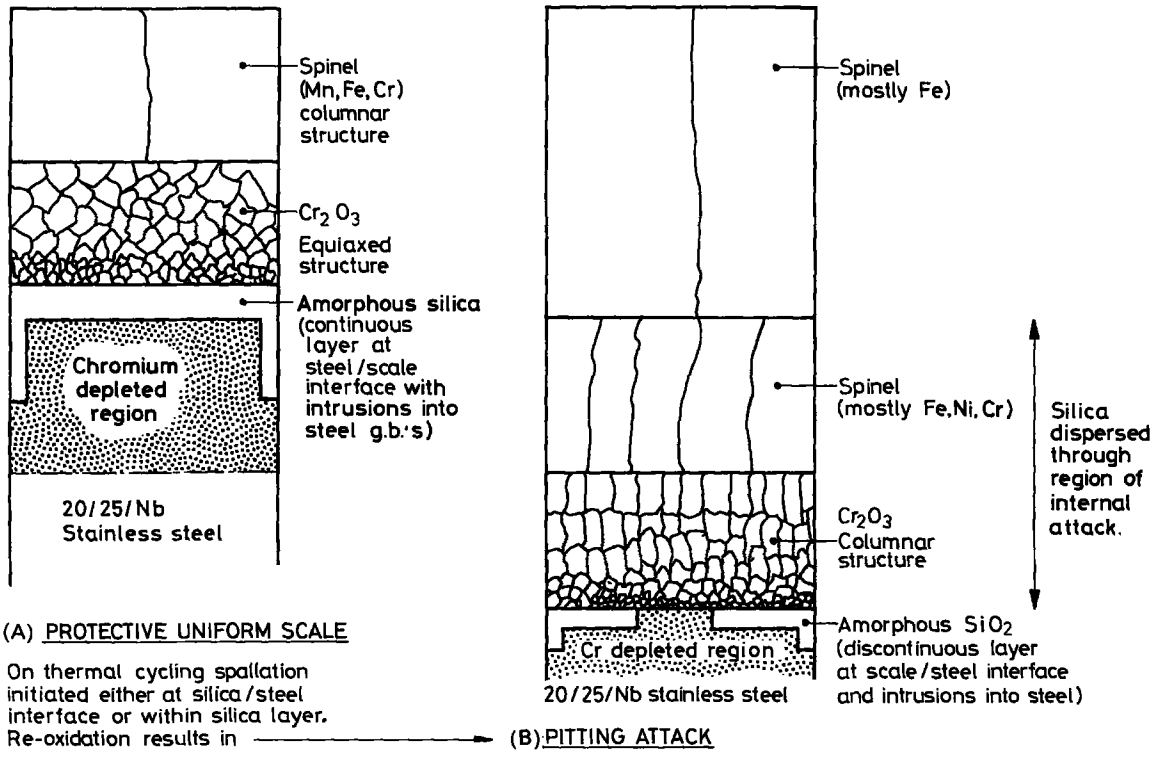

Figure 12 Schematic diagrams showing the fully developed scales formed during the extended oxidation of 20/25/Nb stainless steel in carbon dioxide at 825° C. (A) Protective uniform scale, and (B) region of pitting attack.

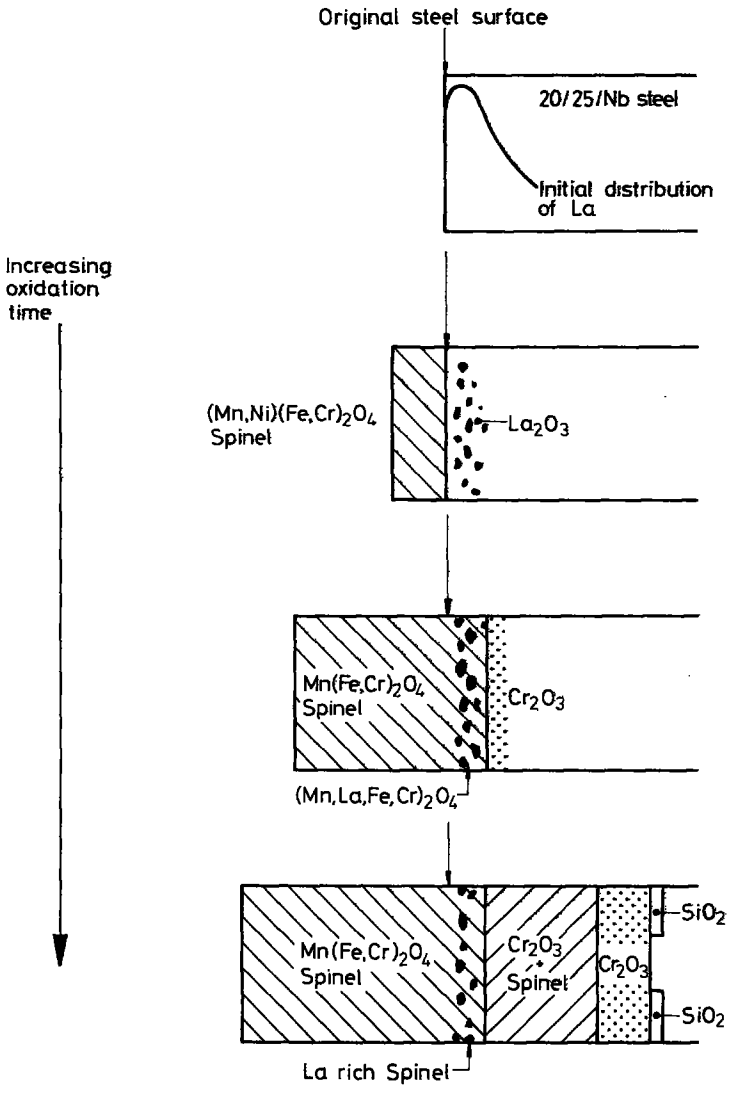

Figure 13 Schematic sequence showing the development of the scale on lanthanum-implanted 20/25/Nb stainless steel during oxidation in carbon dioxide at 825° C.

exposure. Thus, the lanthanum-rich layer acts like a marker for the original surface layer of the steel.

The implanted lanthanum is oxidized more easily than any other constituent of the steel, as in terms of increasing negative free energy of formation of the oxide per mole of oxygen, the sequence is: NiO, Fe_2O_3, Cr_2O_3, MnO, SiO_2, La_2O_3. Therefore, internal oxidation of lanthanum is likely. Based on the above observations, a speculative model to explain the scale growth sequence on lanthanum-implanted 20/25/Nb stainless steel is shown in Fig. 13.

During the initial reaction, a layer of spinel (with cation composition roughly the same as that of the alloy) is formed externally as on the unimplanted 20/25/Nb steel. Thereafter, diffusion leads to increased concentrations of chromium and manganese in the spinel, and internal oxidation of lanthanum beneath the surface. The growing spinel layer thereafter envelopes the La_2O_3 particles and apparently dissolves them to form grains of (Fe, Mn, La, Cr)$_3O_4$. This is surprising in view of the large size of the La^{3+} ion but no diffraction evidence for the rare earth sesquioxide structure could be found.

Soon after the (Mn, Fe, La, Cr)$_3O_4$ layer has been established, the outward diffusion rate of cations decreases and solid state reactions occur between the spinel and the steel substrate, resulting in a manganese/chromium-rich outer spinel oxide and an inner lanthanum/manganese-rich spinel layer. Eventually, a middle duplex oxide layer consisting of Cr_2O_3 and spinel forms, beneath which the inner pure Cr_2O_3 gradually develops. Since the lanthanum acts as a marker, it is apparent that the Cr_2O_3 layer forms by inward growth; i.e. oxygen movement predominates. This may be due either to inward diffusion of oxygen along the Cr_2O_3 grain boundaries or to solid state reactions at the Cr_2O_3/spinel interface. Thus, the role of the lanthanum-rich spinel grains appears to be that of limiting the outward grain-boundary diffusion of cations, thereby changing the growth mechanism of the scale.

The improved adherence of the scale appears to result from its different growth mechanism (i.e. inward as well as outward) and the fact that the SiO_2 layer is discontinuous with the consequence it is no longer a point of fracture. In addition, the large size of the La^{3+} ion may cause trapping of the cation vacancies [7, 8] and hence may reduce the porosity existing inside the scale. Finally, the very small size of the internal scale grains may help to relieve the growth stresses during the formation of the oxide scale [9]. The fine grain size may be due to the internally formed La_2O_3 particles acting to give either a high nucleation rate of the spinel and Cr_2O_3 grains, or a low growth rate of the grains due to grain-boundary pinning. A major consequence of the improved adherence is to prevent pitting attack of the 20/25/Nb stainless steel.

5. Conclusions

Ion-implanted lanthanum is extremely effective in improving the oxidation and spallation resistance of a 20/25/Nb stabilized stainless steel. The implanted lanthanum changes the microstructure of the oxide scale formed. There is no sharp delineation of the innermost Cr_2O_3 and the outermost spinel layers as on the unimplanted 20/25/Nb steel, while the Cr_2O_3 grain sizes are considerably smaller. The presence of the lanthanum also reduces the porosity within the scale. The lanthanum is located in fine spinel grains within a middle layer consisting of both Cr_2O_3 and spinel and at a position close to the interface with the outermost spinel layer. The chemical reactivity and large ionic size of lanthanum are responsible for the modification in the scale growth mechanisms resulting in improved oxidation behaviour.

Acknowledgements

We are grateful for contributions to this study made by G. Dearnaley, J. A. Desport and M. R. Houlton at the Harwell Laboratory, to the CWRU-NSF Materials Research Laboratory for partial support and to TRW, Inc. for a Fellowship (C.H.Y.).

References

1. F. H. STOTT, J. S. PUNNI, G. C. WOOD and G. DEARNALEY, "Ion Implantation Into Metals", edited by V. Ashworth, W. A. Grant and R. P. M. Proctor (Pergamon, London, 1982) p. 245.
2. M. J. BENNETT, B. A. BELLAMY, G. DEARNALEY and M. R. HOULTON, International Congress on Metallic Corrosion Proceedings, Vol. 2, (National Research Council of Canada, Ottawa, 1984) p. 416.
3. J. STRINGER, B. A. WILCOX and R. J. JAFFEE, *Oxid. Metals* **5** (1972) 11.
4. H. M. FLOWER and B. A. WILCOX, *Corros. Sci.* **17** (1977) 253.
5. J. M. FRANCIS and W. H. WHITLOW, *ibid.* **5** (1965) 701.
6. F. A. GOLIGHTLY, F. H. STOTT and G. C. WOOD, *Oxid. Metals* **10** (1976) 163.
7. A. V. SEYBOLT, *Corros. Sci.* **6** (1977) 263.
8. J. K. TIEN and F. S. PETTIT, *Met. Trans.* **3** (1972) 1587.
9. J. E. ANTILL and K. A. PEAKALL, *Corros. Sci.* **16** (1967) 729.
10. M. TINKER and P. A. LABUN, *Oxid. Metals* **18** (1983) 29.
11. M. J. BENNETT, J. A. DESPORT and P. A. LABUN, UKAEA Report, AERE-R11034 (1984); to be published in *Proc. Roy. Soc. (London)*.
12. M. J. BENNETT, M. R. HOULTON and R. W. M. HAWES, *Corros. Sci.* **22** (1982) 111.
13. H. E. EVANS, D. A. HILTON, R. A. HOLM and S. J. WEBSTER, *Oxid. Metals* **14** (1980) 235.

Received 3 February
and accepted 10 April 1986